Journal of Membrane Science 662 (2022) 121022

Contents lists available at ScienceDirect

Journal of Membrane Science

journal homepage: www.elsevier.com/locate/memsci

Controlled biomolecules separation by CO_2-responsive block copolymer membranes

Xiangyue Ye, Jiemei Zhou **, Chenxu Zhang, Yong Wang *

State Key Laboratory of Materials-Oriented Chemical Engineering, College of Chemical Engineering, Nanjing Tech University, Nanjing, 211816, Jiangsu, PR China

ARTICLE INFO

Keywords:
Block copolymer
Responsive membrane
CO_2 response
Selective swelling
Biomolecule separation

ABSTRACT

The intelligent responsive membranes have aroused much attention due to their distinctive capability to reversibly change separation performances under the stimulation of ambient environment. Especially, the responsive membranes derived from block copolymers, which have regular nanoporous structures, display great potential in high-precision controllable separation. Herein, we use CO_2 gas as the non-toxic, mild stimulus, and develop the responsive membranes from a block copolymer of poly(2-diethylaminoethyl methacrylate)-block-polystyrene (PDEAEMA-*b*-PS) by the selective swelling method. The membranes exhibit a bi-continuous nanoporous structure and the surfaces and pore walls are rich with CO_2-responsive PDEAEMA chains. Based on the reversible conformation transition of PDEAEMA chains between the collapsed state and extended state upon CO_2/N_2 stimulation, the membranes achieve the controllable regulation on the water permeances from ~100 to ~2100 $L{\cdot}h^{-1}{\cdot}m^{-2}{\cdot}bar^{-1}$, also realize the blocking/passing switch for varied proteins. More importantly, the extended PDEAEMA chains shrink the effective pore size down to less than 5 nm, moving the separation scope from ultrafiltration to tight-ultrafiltration. Thus, the membranes are capable to separate macromolecular proteins with small molecule polypeptide and vitamin with high separation efficiencies, demonstrating their application prospect in precise separation and fractionation of biomolecules.

1. Introduction

The responsive membranes are a new generation of smart membranes developed based on bionic materials [1]. They are mainly composed of porous base membranes and exterior functional polymers that can sense external stimulus. The chemical structure, property or conformation of exterior polymers can be changed with the physical and/or chemical factors in the external environment (such as temperature [2,3], pH [4,5], magnetic field [6], electric field [7] and light [8], etc.), resulting in changes of the effective pore size and permeability of membranes [9,10]. Due to the intelligent feature, the responsive membranes become a hot topic in the field of membrane research and show great potential applications in control release [11], biological separation [12], chemical sensors [13], water treatment [14,15] and many other fields [16,17].

Generally, the approaches to prepare responsive membranes usually can be divided into two types [18]. The first is to modify the existing membranes with stimuli-responsive polymers by grafting [19], adsorption [20] or filling [21]. It can be used to transform the commercial membranes into the smart membranes. However, this approach is difficult to guarantee the full coverage and evenness of the modification on the interior walls of membranes, and the smaller the membrane pores are, the more difficult the modification is. Thus this approach is more effective for the modification of microporous membranes, but resulted membranes are not suitable for the separation of nano-scale substances. The other is to use stimuli-responsive polymers as raw materials in membrane formation. For example, Kobayshi et al. [22] synthesized a copolymer by random copolymerization of acrylic acid, methacylic acid and acrylonitrile, and use it to prepare the pH-responsive polyacrylonitrile ultrafiltration membranes by phase inversion. Grafting modification on traditional polymer materials, such as polyvinylidene fluoride (PVDF) [23] and polyethersulfone (PES) [24], so as to introduce responsive polymers into the side chains has also been commonly used for the preparation of various smart membranes. This approach usually guarantees the uniform modification of the whole membranes, however the regularity of pore structures is still an issue in need of improvement, which restricts their applications in controlled precise separation.

Block copolymers (BCPs) recently show great advantages as the

* Corresponding author.
** Corresponding author.
E-mail addresses: zhoujm@njtech.edu.cn (J. Zhou), yongwang@njtech.edu.cn (Y. Wang).

https://doi.org/10.1016/j.memsci.2022.121022
Received 30 June 2022; Received in revised form 8 August 2022; Accepted 15 September 2022
Available online 19 September 2022

candidate to prepare the intelligent responsive membranes. Profited from the specific property of microphase separation, BCPs can form the membranes with high regularity in structure and pore sizes, in which the majority blocks constitute the porous matrix and the minority blocks are evenly enriched on the surfaces and pore walls. Using the minority block containing responsive groups can consequently give the stimuli-responsive membranes. Our group prepared the pH-responsive membranes from poly(2-vinylpyridine) (P2VP) based block copolymers by selective swelling and investigated their regulation on water fluxes with the variation of pH [25]. Qiu et al. [26] reported the membrane with uniform pore sizes prepared by combining the self-assembly of the block copolymer polystyrene-block-poly(4-vinylpyridine) (PS-*b*-P4VP) with nonsolvent-induced phase separation. By changing the charge properties of the membrane through adjusting the external pH, separation of two similar-sized proteins can be realized. The nanostructure, narrow pore size distribution and perfect coverage of the responsive polymer layer on interior walls of BCP-derived membranes make them extremely fit for the applications in the fields of responsive release and exquisite fractionation of biomolecules, whereas the relevant researches about them are rare so far.

In term of constructing a responsive membrane system, the introduction of external stimulus is necessary. Among the multitudinous stimulus, CO_2 gas has attracted special attentions due to its advantages of low price, abundance, non-toxicity, mild response conditions and no salt accumulation in the system [27]. CO_2 stimulation response only needs to bubble CO_2 or N_2/Ar gas into the system to achieve the reversible regulation on the membrane performances. It would not change the chemical structure, conformation or cause deactivation of proteins, especially suitable for the biomolecules system. The potential applications of CO_2-responsive membranes in protein separation can be considered from two aspects. First, in circumstances where CO_2 are involved, for example, fermentation, the responsive membranes may be used to separate specific proteins smartly regulated by the concentration of CO_2 intrinsically present and dynamically changed in the separation systems. Second, CO_2 can be purposely introduced into the separation systems to tune the effective pore sizes and surface properties of the responsive membranes in accordance to the real-time characteristics of the separation systems, thus maximizing the separation performances. Zhang et al. [28] immobilized CO_2-responsive microgels in commercial microfiltration membranes by adsorption to prepare CO_2-responsive membranes. The shrinkage and expansion of microgels under alternate bubbling of N_2/CO_2 realized the change in water fluxes. Zhao et al. [10] grafted poly(2-diethylaminoethyl methacrylate) (PDEAEMA) on the surface and pore walls of polyvinylidene fluoride (PVDF) membranes, which endowed the latter with CO_2 responsiveness. The mean pore size of prepared membranes was gas-tuneable between 162 and 60 nm, achieving the controllable rejection for gold nanoparticles. These studies have demonstrated the efficiency of CO_2 stimulation response to reversibly regulate the membrane performances. However, less effort has been made to develop the CO_2 stimuli-responsive separation membranes with satisfying pore size range for protein separations and their applications in biomolecules system. Therefore, in this work we synthesized a BCP of poly(2-diethylaminoethyl methacrylate)-block- polystyrene (PDEAEMA-*b*-PS) by reversible addition-fragmentation chain transfer (RAFT) polymerization, and used it as the raw material to fabricate the CO_2-responsive ultrafiltration membranes by the process of selective swelling-induced pore generation, then applied the membranes to biomolecules separation. The PDEAEMA chains are inherently hydrophobic and exhibit a collapsed chain conformation, while upon exposure to CO_2 in water, the tertiary amine groups of PDEAEMA chains can react with CO_2 to form the protonated state, which makes PDEAEMA hydrophilic and presents an extended chain conformation. The PDEAEMA chains act as the gates of the membranes pores, the CO_2/N_2 treatment regulates the on-off switch, thus realizing the intelligent control on the protein-passing channels. Compared with our previous reported CO_2-responsive membranes [29], the PDEAEMA-*b*-PS membranes realize the regulation on surface hydrophilicity-hydrophobicity transition and have the wider adjusting range in pore size and permeance. Upon the presence of CO_2, the extended PDEAEMA chains could shrink the pore size down to less than 5 nm, moving the membrane from ultrafiltration to tight-ultrafiltration, which is hard to be achieved for BCP membranes without the aid of post-modification or additives [30,31]. With a small pore size of 4.2 nm and corresponding molecular weight cut-off (MWCO) of 8380 Da, the membranes can be utilized to effectively separate mixed biomolecules, such as bacitracin/lysozyme with a high separation efficiency of 97%.

2. Experimental section

2.1. Materials

2-Diethylaminoethyl methacrylate (DEAEMA, 99%) and styrene (>99%) were purchased from Aladdin and Energy, respectively. Prior to use, we removed inhibitors by passing them through basic alumina columns, then stored in the refrigerator (−20 °C). 2, 2′-Azobis (isobutyronitrile) (AIBN, 98%) was purchased from Aladdin and further purified by recrystallization from ethanol. 2-Cyano-2-propyl benzodithioate (CPBD, >97%) and tetrahydrofuran (THF, ≥99.9%) were purchased from Aladdin and used without further purification. Macroporous polyvinylidene fluoride (PVDF) membranes (25 mm in diameter, 0.22 μm in average pore size) were ordered from Millipore and served as substrates to prepare ultrafiltration composite membranes. Bovine serum albumin (BSA) and bovine hemoglobin (BHb) were sourced from MP Biomedicals Co., Ltd and Shanghai Yuanye Bio-Technology Co., Ltd, respectively. Lysozyme and myoglobin were purchased from Sigma-Aldrich. Bacitracin and vitamin B12 (VB-12) were purchased from Macklin. CO_2 (>99.9%) and N_2 (>99.999%) were purchased from Nanjing Shangyuan Industrial Gas Factory. All other chemical reagents being of analytical grade such as acetonitrile, ethanol, chloroform, etc. were provided by Sinopharm and Aladdin. Silicon wafers were thoroughly washed several times with ethanol under ultrasonication before use. Deionized water used in all experiments was lab-made with the conductivity of 8–20 $\mu s \cdot cm^{-1}$.

2.2. Synthesis of PDEAEMA-b-PS

Scheme S1 shows the synthetic route of PDEAEMA-*b*-PS. Typically, a 50 mL polymerization tube with a magnetic bar was used as the reaction vessel. DEAEMA (12.4875 g, 45 mmol), CPDB (99.45 mg, 0.3 mmol), AIBN (14.76 mg, 0.06 mmol) and THF (12 g) were mixed and placed into the tube. After being degassed through three freeze-pump-thaw cycles, the tube was sealed and placed into an oil bath of 70 °C. After 24 h, the reaction was stopped by cooling the tube to room temperature and exposing the polymer solution to air. The polymer solution was precipitated into excess acetonitrile three times to remove unreacted monomers. Finally, the solid polymer was collected and placed in a vacuum oven at room temperature for drying.

The obtained polymer of PDEAEMA was used as the macro-chain transfer agent (macro-CTA) for the subsequent BCP synthesis, and the procedure is as follows: PDEAEMA (400 mg, 0.02 mmol), styrene (4.16 g, 40 mmol) and AIBN (0.524 mg, 0.0032 mmol) was dissolved in methanol (2.4 g), then the solution was added into a 20 mL polymerization tube with a magnetic bar. Similar to the previous step, the tube was degassed and sealed, then put into a preheated oil bath at 80 °C for 48 h polymerization. Finally, the polymer solution was precipitated into excess acetonitrile three times for purification, followed by drying completely at 45 °C under vacuum to obtain the product.

2.3. Preparation of nanoporous PDEAEMA-b-PS thin films/membranes

PDEAEMA-*b*-PS was ultrasonically dissolved in chloroform with a concentration of 2 wt%, and the polymer solution was filtrated through

a polytetrafluoroethylene (PTFE) filter (0.22 μm in average pore size) three times to remove any impurities thoroughly. The solution was spin-coated on clean silicon substrates at 2000 rpm for 30 s to prepare PDEAEMA-*b*-PS thin films. Subsequently, the films were soaked in ethanol at 65 °C to conduct selective swelling process. After desired durations, the films were withdrawn from ethanol and dried naturally.

PDEAEMA-*b*-PS composite membranes were then prepared using PVDF membranes as the substrates. Specifically, the PVDF membranes were first soaked in deionized water for 20 min to fill the pores in order to prevent downward percolation of the polymer solution during the subsequent spin coating process. The PVDF membranes filled with water were placed on clean glass slides, using papers to absorb excess water on the surface. Then, the above-prepared polymer solution was spin-coated on PVDF membranes at 2000 rpm for 30 s to form thin BCP layers. Subsequently, the membranes were placed in an oven at 60 °C for 15 min to make the water and solvent evaporate completely. Finally, the membranes were immersed in ethanol at 65 °C to produce nanoporous structures in BCP layers.

2.4. Characterization

The chemical structures of polymers were characterized on a nuclear magnetic resonance spectrometer (NMR, AV400, Bruker) using $CDCl_3$ or D_2O as the solvent, tetramethylsilane (TMS) as internal standard. The thicknesses and refractive indices of BCP thin films on silicon wafers were recorded via a spectroscopic ellipsometer (Complete EASE M-2000U, J. A. Woollam). The porosities can be calculated based on the refractive index values using the following Eq. (1):

$$n_p^2 = n_0^2\left(1-\varphi_{pore}\right) + n_{air}^2\varphi_{pore} \tag{1}$$

where n_{air} represents the refractive index of air with a value of 1, n_0 and n_p are the refractive indices of the dense and porous films, respectively. φ_{pore} represents the porosity of the thin film.

A field-emission scanning electron microscopy (FESEM Hitachi S4800) was used to observe the surface and cross-sectional morphologies of BCP films and composite membranes at an operation voltage of 3 kV. Cross-sectional observation should immerse samples in liquid nitrogen for 10 s and quickly fracture them to expose the cross sections. All samples were sputter-coated with a thin layer of Au to enhance conductivity for achieving clear images. Surface hydrophilicity was evaluated by analyzing under oil water contact angle (UOWCA) [32] utilizing a contact angle measurement device (Dropmeter A100, Maist). We injected n-heptane into the sample cell and placed the film face down below the liquid surface of n-heptane, then injected 5 μL of water with the injection probe to test the water contact angle of the membrane surface in n-heptane. Gel permeation chromatography (GPC) analysis was performed with a Waters 1515 chromatograph system to evaluate the MWCO of membranes. The zeta potential of the membrane surface was analyzed via an electrokinetic analyzer (SurPASS, Anton Paar, Austria) using 1 mmol/L potassium chloride (KCl) aqueous solution as an electrolyte environment.

2.5. Filtration experiments

We used a homemade dead-end filtration device (Fig. S2) with an actual filtration area of 3.14 cm^2 to evaluate the separation performances of BCP composite membranes under gentle CO_2/N_2 stimulation. Prior to the experiment, the membrane was pressurized at 0.5 bar for 10 min to ensure a steady filtration state. Then we bubbled CO_2 into the feed solution for 3 min or bubbled N_2 for 10 min to conduct the stimulation. In order to better control the gas flow rate, we installed a needle tube at the gas inlet, and controlled the gas valve switch to ensure that the gas slowly entered into the feed solution. All tests were executed by using three-parallel membranes to obtain reliable data. The water volume passing through the membrane was recorded, and the pure water permeance (*Perm*) was calculated by Eq. (2):

$$Perm = \frac{V}{A\cdot t\cdot \Delta p} \tag{2}$$

where V (L) is the water volume, A (m^2) represents the effective area of the test membrane, t (h) is the permeating time and Δp (bar) represents the operation pressure.

Dextrans with diverse molecular weights of 10, 40, 70 and 500 kDa were mixed and dissolved in deionized water with the concentration for each component of 2.5, 1, 1 and 2 g/L, respectively. The mixed dextran solution was utilized to measure the MWCO of membranes by filtration. The dextran concentrations in feed and filtrate were determined by GPC analysis, and the effective pore size of membranes can be calculated by Eq. (3):

$$r = 0.33M_w^{0.46} \tag{3}$$

where r (Å) is the effective pore radius of membranes and M_w (Da) is the MWCO of dextran.

The rejection tests were conducted with the same filtration device under gentle CO_2/N_2 stimulation. The aqueous solutions of BSA, BHb, myoglobin, lysozyme, bacitracin and VB-12 with a concentration of 0.5 g/L were used as the feed solutions. After filtration by membranes, by using the UV–vis absorption spectrometer (NanoDrop 2000C, Thermo Fisher), the concentrations of BHb, myoglobin, bacitracin, and VB-12 in feed and filtrate were analyzed at 406 nm, 409 nm, 229 nm, and 520 nm, respectively. The concentrations of BSA and lysozyme were obtained at 280 nm in the "protein A280″ model of the UV–vis absorption spectrometer. The rejection ratio (R) can be calculated by Eq. (4):

$$R = \frac{C_f - C_p}{C_f} \times 100\% \tag{4}$$

where C_f and C_p represent the concentrations (g/L) in feed and filtrate, respectively.

The mixtures of two substances with different sizes (myoglobin and VB-12, myoglobin and bacitracin, lysozyme and VB-12, lysozyme and bacitracin, 0.5 g/L for each one) were used to evaluate the size screening capability of membranes under CO_2 stimulation. The selective separation efficiency (*SE*) can be determined by Eq. (5) [33]:

$$SE = \frac{C_{small\ molecule}}{C_{protein} + C_{small\ molecule}} \times 100\% \tag{5}$$

where $C_{prorein}$ and C_{small} molecule represent the protein concentration and small molecule concentration in filtrate, respectively.

3. Results and discussion

3.1. Synthesis of PDEAEMA-b-PS

The PDEAEMA homopolymer was synthesized via RAFT polymerization, then used as the macro-CTA for the synthesis of PDEAEMA-*b*-PS. 1H NMR characterizations were used to verify the chemical structures of obtained polymers. As shown in Fig. S3, all characteristic peaks of PDEAEMA and PDEAEMA-*b*-PS are marked out in the spectra, confirming the successful synthesis of target products. Based on the signals of phenyl protons in the CPBD group at 7.35–7.90 ppm and the signals of ester methylene protons in DEAEMA units at 4.01 ppm, the degree of polymerization (DP) of PDEAEMA was calculated to be 130. According to the signals of phenyl protons in styrene units appearing at 6.20–7.24 ppm and the signal at 4.01 ppm, the DP of PS was determined to be 590. Therefore, it was obtained that the molecular weight of PDEAEMA was 24.1 kDa, and the molecular weight of PS was 61.4 kDa, so the mass fractions of PDEAEMA and PS blocks were 28.2% and 71.8%, respectively. The BCP with this block weight ratio can theoretically form a bicontinuous porous structure according to previous studies [34].

3.2. Nanoporous PDEAEMA-b-PS films prepared by selective swelling

Selective swelling is a powerful method to produce nanoporous structures in BCPs [35]. In order to use this method to prepare membranes, we first explored the swelling behaviors of PDEAEMA-*b*-PS which hasn't been studied before. Ethanol can dissolve the PDEAEMA homopolymer very well in experiment while is a poor solvent for the PS homopolymer, that is, it is a selective solvent for the PDEAEMA block in PDEAEMA-*b*-PS. Therefore, we used ethanol as the swelling agent and the selective swelling process was conducted as shown in Fig. 1.

The PDEAEMA-*b*-PS thin films were prepared by spin coating and then were immersed in ethanol at 65 °C for different durations. The surface and cross section of the original film were dense and non-porous, as displayed in Figs. S4a–b. After swelling, the films all exhibited nanoporous structures, but different morphologies can be observed under different durations (Figs. 2 and S4). For the film subjected to 1 h swelling, some round and elongated pores appeared on the surface (Fig. 2a), but most area was still dense. When the swelling duration was prolonged to 2 h, more pores were formed, thus the dense area became less (Fig. S4c). When the swelling duration was 5 h, the bi-continuous porous structure was basically formed (Fig. 2b). Then further lasting the swelling durations to 10 h and 20 h, the films kept similar morphologies, but the pore sizes were enlarged (Figs. S4e and 2c). The cross-sectional view of films manifested the formed pores penetrated the whole film thickness whatever the swelling durations.

Ellipsometry tests recorded the thickness change of films during swelling (Fig. 3a). The thicknesses of films were increased sharply from initial 280 nm–425 nm in the first 1 h, then slowly increased to 450 nm, 465 nm, 480 nm, 510 nm at 2 h, 5 h, 10 h and 20 h, respectively. In addition to the thickness change, the refractive indices of films were apparently dropped because of the formation of large amounts of pores. The porosities were determined according to Eq. (1), which were 42%, 47.3%, 48.3%, 50.3%, and 52.9%, respectively, as presented in Fig. 3b. Besides, we calculated the surface pore sizes of films from SEM images (Figs. 2 and S4) using Nano Measurer software. With the increase of swelling durations from 1 h to 20 h, the pore sizes were determined to be 38 nm, 42 nm, 44 nm, 45 nm, 52 nm, respectively.

According to our previous study about selective swelling [35], the swelling process of PDEAEMA-*b*-PS films can be described as follows: ethanol preferentially enters the PDEAEMA phase because of the strong affinity between ethanol and PDEAEMA chains, causing the PDEAEMA domains to expand their volumes, and at the same time PS phases are squeezed to undergo plastic deformation. When films are taken out from the swelling agent, the solvent volatilizes and the PDEAEMA chains collapse and attach on the film surface and pore walls, at the same time, nanopores are formed [36–38]. The swelling duration effects the swelling degree of PDEAEMA domains, consequently the pore size. Therefore, the longer swelling duration generally give rise to the larger pore size, as we observed above.

The tertiary amine groups in PDEAEMA chains of PDEAEMA-*b*-PS films can react with CO_2 in water to form ammonium bicarbonate, making the chains protonated, thus changing the chain conformation in water [39,40]. In regard to the PDEAEMA-*b*-PS films, the conformation transformation of PDEAEMA chains attached on the film surface may lead to the change in film thickness (Fig. 4a). Therefore, we utilized the liquid cell function of ellipsometer to monitor the film thickness value in situ upon CO_2 bubbling, as Fig. 4b shows. The PDEAEMA-*b*-PS film prepared by 5 h swelling was selected as the sample. The film in the dry state had a thickness of 459 nm. When the film was locked in the liquid cell and deionized water was injected, the film thickness had a slight increase and stabilized at 463 nm ultimately. This is because the film was swelled due to water absorption, also a very small part of CO_2 gas dissolved in deionized water made PDEAEMA protonated. Then CO_2-saturated water was injected in the liquid cell, and the film thickness was rapidly increased to 511 nm in half an hour. The whole test process lasted for 2 h, and the film thickness maintained at about 515 nm at the end, increased by 52 nm in contrast with the one before the CO_2 stimulation. The phenomenon of the thickness increase evidenced the conformation transformation of PDEAEMA chains from the collapsed state to the stretched state, also suggested that the conformation transformation was mainly caused by the CO_2 stimulation, rather than water swelling.

In addition to chain conformation, the hydrophilicity of PDEAEMA can also be changed by the CO_2 stimulation. We dissolved the PDEAEMA polymer in water, but only got a cloudy solution (Fig. S5a), indicating PDEAEMA is inherently hydrophobic. The solution turned into a clear one after bubbling CO2 in it (Fig. S5b), this showed that the PDEAEMA chains became hydrophilic due to the protonation by CO2. The hydrophilicity-hydrophobicity transition of PDEAEMA chains under CO_2 stimulation would surely affect the surface property of the PDEAEMA-*b*-PS film. Therefore, we evaluated the surface hydrophilicity change of the film in response to CO_2/N_2 by the UOWCA performance, as presented in Fig. 4c. The WCA on the surface of the original film basically stabilized at about 139°. After CO_2 stimulation, the WCA was decreased to 88°, owing to the protonation of PDEAEMA chains on the film surface. Subsequently, N_2 was introduced into the system to make CO_2 gas escape, and the quaternary amine groups in PDEAEMA underwent deprotonation reversibly going back to tertiary amines, as a result,

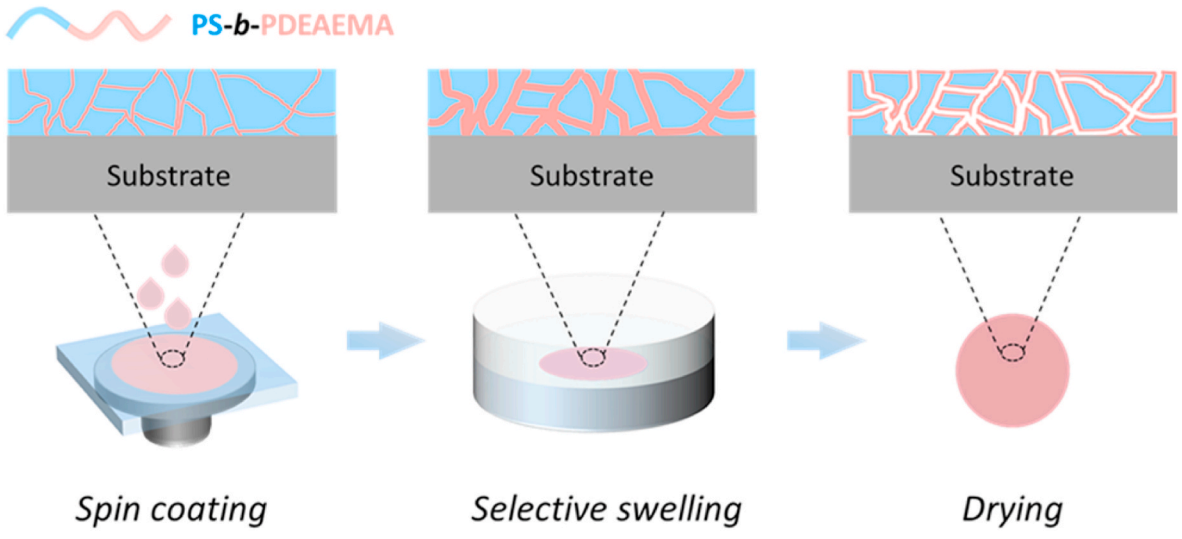

Fig. 1. Schematic of the selective swelling process.

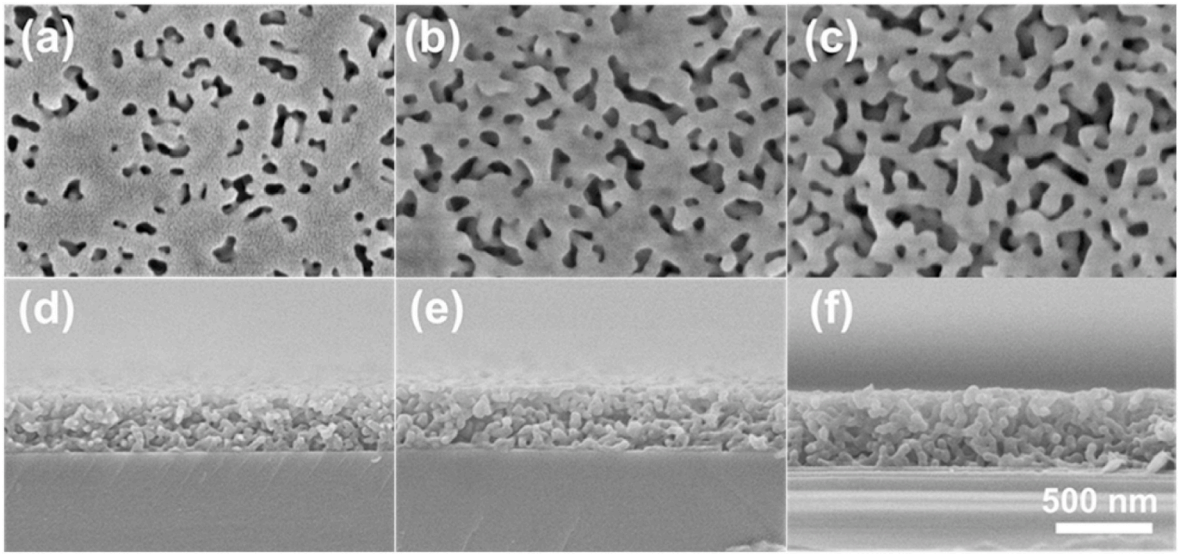

Fig. 2. (a–c) The surface and (d–f) cross-sectional SEM images of PDEAEMA-*b*-PS films immersed in ethanol at 65 °C for different durations: (a, d) 1 h, (b, e) 5 h, (c, f) 20 h. All images have the same magnification, and the scale bar corresponding to 500 nm is shown in (f).

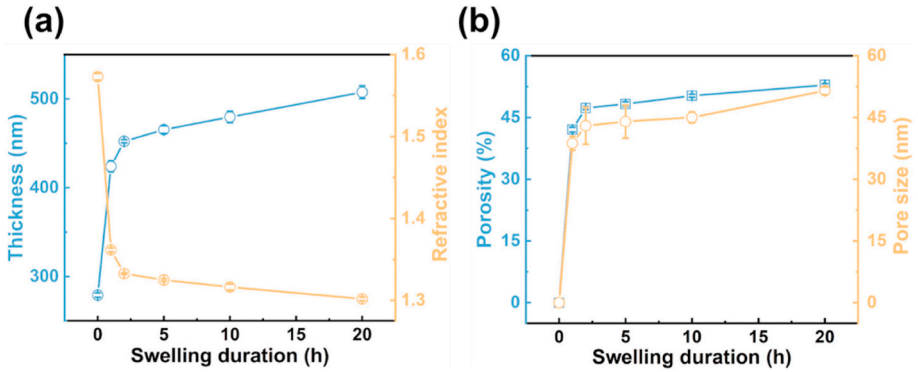

Fig. 3. (a) The thicknesses and refractive indices of films for different swelling durations. (b) The porosities and pore sizes of films corresponding to swelling durations.

the WCA returned to about 130°. CO_2/N_2 stimulation displayed the regulation on Apparently, the surface hydrophilicity of the film can be effectively regulated by manipulating the CO_2/N_2 treatment.

3.3. Separation performances of PDEAEMA-b-PS membranes

As the CO_2 responsiveness of PDEAEMA-*b*-PS thin films was proved above, we prepared the PDEAEMA-*b*-PS composite membranes by coating the PDEAEMA-*b*-PS layer on the macroporous substrate. The PDEAEMA-*b*-PS layer with a nanoporous structure (Fig. 5a–b) plays the role of sieving and determines the responsibility. The swelling durations were changed from 1 h, 2 h, 5 h, 10 h, to 20 h to tune the pore size of PDEAEMA-*b*-PS layers, and the pure water permeances were evaluated upon CO_2/N_2 bubbling. As shown in Fig. 5c, the permeances gradually rose with the increase of swelling durations under N_2 bubbling because of the enlarged pore sizes. The water permeance of the composite membrane swollen for 1 h was about 1194 $L{\cdot}m^{-2}{\cdot}h^{-1}{\cdot}bar^{-1}$. For the swelling durations of 2 h and 5 h, the permeances were increased to 1607 and 1924 $L{\cdot}m^{-2}{\cdot}h^{-1}{\cdot}bar^{-1}$, respectively. Further prolonging the swelling durations to 10 h and 20 h, the permeance showed a slight decrease, stabilizing at about 1800 $L{\cdot}m^{-2}{\cdot}h^{-1}{\cdot}bar^{-1}$, although the porosity and pore size should be increased. This may be because the porous structure with a high porosity was relatively loose, it occurred a certain degree of compaction under test pressure. When the water permeances were tested under CO_2 bubbling, the PDEAEMA chains were transformed from hydrophobic to hydrophilic, and the PDEAEMA chains attached on pore walls were fully stretched and filled in the pores, consequently the permeances dropped sharply. With the swelling durations of 1 h, 2 h, 5 h, 10 h and 20 h, water permeances of composite membranes were 47, 101, 104, 114, 100 $L{\cdot}m^{-2}{\cdot}h^{-1}{\cdot}bar^{-1}$, respectively. It can be noticed from Fig. 5c that the permeance difference of the membrane swelled for 5 h upon CO_2/N_2 bubbling was the largest, therefore we chose this composite membrane as the best sample to do the cyclic test. As presented in Fig. 5d, N_2 was first introduced to the system. Then, CO_2 was bubbled to change the conformation of PDEAEMA chains and narrow down the pores, and the permeance was decreased by 94%. Subsequently bubbling N_2, the water permeance returned to the initial level, confirming the reversible variation of the pore size for the PDEAEMA-*b*-PS membrane. The membrane exhibited controlled switching in water permeance between ~2100 and ~100 $L{\cdot}m^{-2}{\cdot}h^{-1}{\cdot}bar^{-1}$ for five test cycles of alternating bubbling of CO_2 and N_2, displaying great cyclic responsiveness and stability.

Based on the controllable regulation on pore size upon CO_2/N_2 stimulation, we explored the application of PDEAEMA-*b*-PS membranes in the separation of biological substances. The membrane prepared by 5 h swelling was used for experiments. First, four proteins with different size and charges were selected as models, and their detailed characteristics are summarized in Table 1. Proteins of BSA and BHb have similar

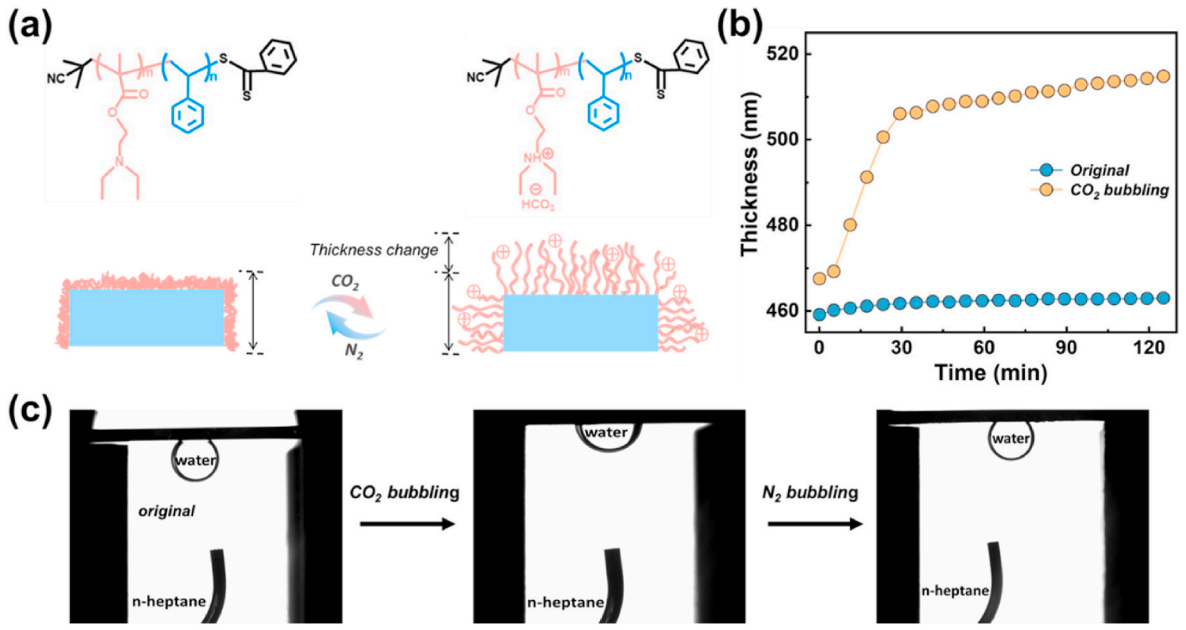

Fig. 4. (a) The mechanism of the film thickness increase by CO_2 bubbling. (b) The thickness change of the PDEAEMA-*b*-PS film in water by CO_2 bubbling. (c) The UOWCA of the PDEAEMA-*b*-PS film under CO_2/N_2 stimulation.

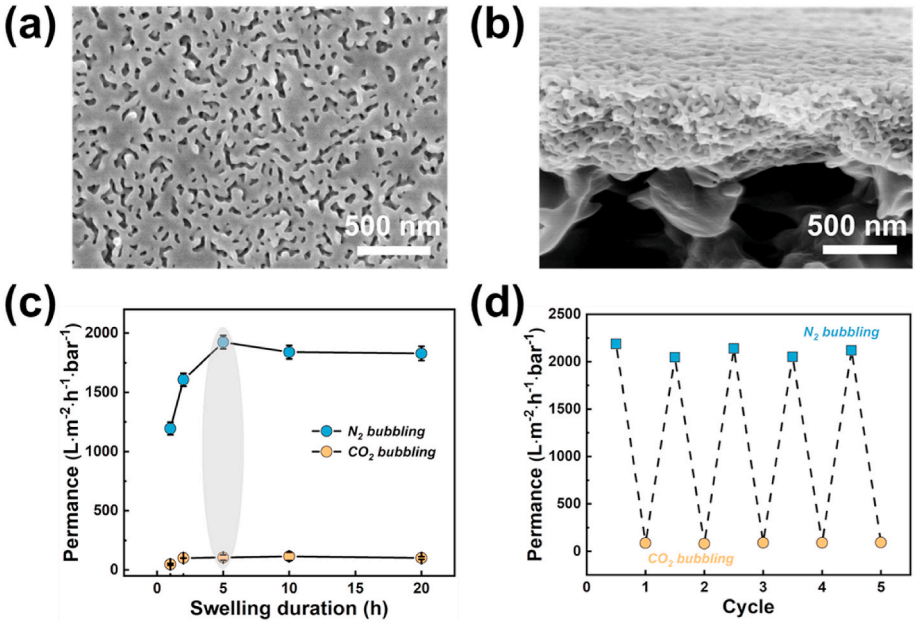

Fig. 5. (a) The surface and (b) cross-sectional SEM images of the PDEAEMA-*b*-PS membrane prepared by swelling in ethanol at 65 °C for 5 h. (c) The permeances of membranes corresponding to swelling durations under CO_2/N_2 bubbling. (d) The reversible permeance switchability of membranes.

molecular weights, which are much larger than other proteins. Upon the presence of CO_2, stretched PDEAEMA chains filled in the pores, thus the rejections of membranes to BSA and BHb were tested to be 90% and 98%, respectively as shown in Fig. 6a. The MWCO of the membrane in this state was measured to be 8380 Da (Fig. S6). Based on the MWCO value and Eq. (3), the effective pore size of the membrane was determined to be 4.2 nm, which is lower than the sizes of BSA and BHb, therefore, the high rejections to the two proteins were achieved depending on size sieving. Especially, the rejection to BHb is approaching 100%, which is higher than BSA although they have similar molecular weights. This is because BSA is a prolate ellipsoid [49] with a three dimensional size of 14 nm × 3.8 nm × 3.8 nm, while BHb is nearly spherical in shape [50] with a size of 6.4 nm × 5.5 nm × 5 nm. When the ellipsoidal BSA molecules align the long axis perpendicular to the membrane pores, they have the chances to percolate through the pores, comparatively the BHb molecules can be intercepted regardless of the alignment. When removing CO_2 by bubbling N2, PDEAEMA chains were switched to the collapse state and the pore size were broadened to about 44 nm based on the SEM image in Fig. 5a. The rejections to BSA and BHb were decreased to 40% and 63%, respectively. The proteins of lysozyme and myoglobin have medium molecular weights, while the MWCO of the membrane under CO_2 stimulation is still smaller than their molecular weights, consequently we also got high rejections to lysozyme and myoglobin, 98% and 91%, respectively. Besides the size sieving effect, electrostatic repulsion contributes to the rejection result of lysozyme as well. The membrane surface is positively charged in the presence of CO_2

Table 1
Summary of properties of used biomolecules as separation models.

Separation target	**Molecular weight (kDa)**	Size	Isoelectric point	Ref.
BSA	67	14 nm × 3.8 nm × 3.8 nm	4.7	[31, 39]
BHb	65	6.4 nm × 5.5 nm × 5 nm	7.0	[31,41, 42]
myoglobin	17	4.5 nm × 3.5 nm × 2.5 nm	7.1	[33, 43]
lysozyme	14.3	1.9 nm × 2.5 nm × 4.3 nm	11.0	[44, 45]
bacitracin	1.42	2.8 nm × 1.3 nm	8.8	[46, 47]
VB-12	1.35	1.7 nm × 1.8 nm	–	[48]

(Fig. S7), and lysozyme with an isoelectric point of 11.3 is also positively charged. The repulsive interaction between the same charges results in the nearly 100% rejection to lysozyme. By contrast, myoglobin is electrically neutral and cannot form charge repulsion, so the rejection of membrane to it is lower than lysozyme. Removing CO_2 to open the pores of membrane, the rejections to lysozyme and myoglobin were decreased to 51.4% and 30%, respectively. To investigate the reversibility of the selectivity performance of membranes, we did the cyclic tests of rejections to BSA under alternating CO_2/N_2 bubbling. From the results shown in Fig. 6b, the membrane could maintain almost the same rejection to BSA after five cycles, demonstrating the great cyclic responsiveness in selectivity performance.

Evidently, the PDEAEMA chains work like the gate of the membrane pores, the response to CO_2/N_2 bubbling regulates the turn off or turn on of the protein transport channels (Fig. 6c). We know proteins are large molecules with the molecular weight range of about 6000 Da to millions. The biological substances with the molecule weight less than 6000 Da, such as polypeptide and vitamin, belong to small molecules. The MWCO of the membrane under CO_2 stimulation approaches the demarcation between large and small molecules. Therefore, the membrane theoretically can intercept most of the large protein molecules, but allow small molecules to pass through, enabling the screening of biological substances. The interception of proteins has been demonstrated by four different proteins as discussed above. We further explored the rejections to bacitracin and VB-12. As shown in Fig. 6a, under the CO_2 and N_2 stimulation, the rejections to bacitracin by the composite membrane were 21.5% and 9.9%, respectively, owing to its small size with a molecular weight of 1422 Da. Similarly, for the small molecule VB-12, the rejections were lower than 10% under the CO_2 and N_2 stimulation.

According to the above, macromolecular proteins are rejected, while small molecular substances can pass through the membrane pores upon CO_2 stimulation. Therefore, we further used the membrane to separate mixed substances because the mixture separation efficiency is a crucial parameter for practical applications. We selected four mixtures of VB-12/myoglobin, bacitracin/myoglobin, VB-12/lysozyme and bacitracin/lysozyme for tests, and the UV–vis spectra before and after filtration are shown in Fig. 7a–d. For the mixtures of VB-12/myoglobin, bacitracin/myoglobin, the spectral intensities of myoglobin were significantly decreased in filtration because of the rejection effect by the membrane, while those of VB-12 and bacitracin still displayed high intensities. In terms of the mixtures of VB-12/lysozyme and bacitracin/lysozyme, the intensities of lysozyme decreased to nearly zero, while the spectra of VB-12 and bacitracin remained almost unchanged. These results demonstrated the effective separation of different biomolecules. Furthermore, we calculated the selective separation efficiencies for VB-12/myoglobin, bacitracin/myoglobin, VB-12/lysozyme and bacitracin/lysozyme

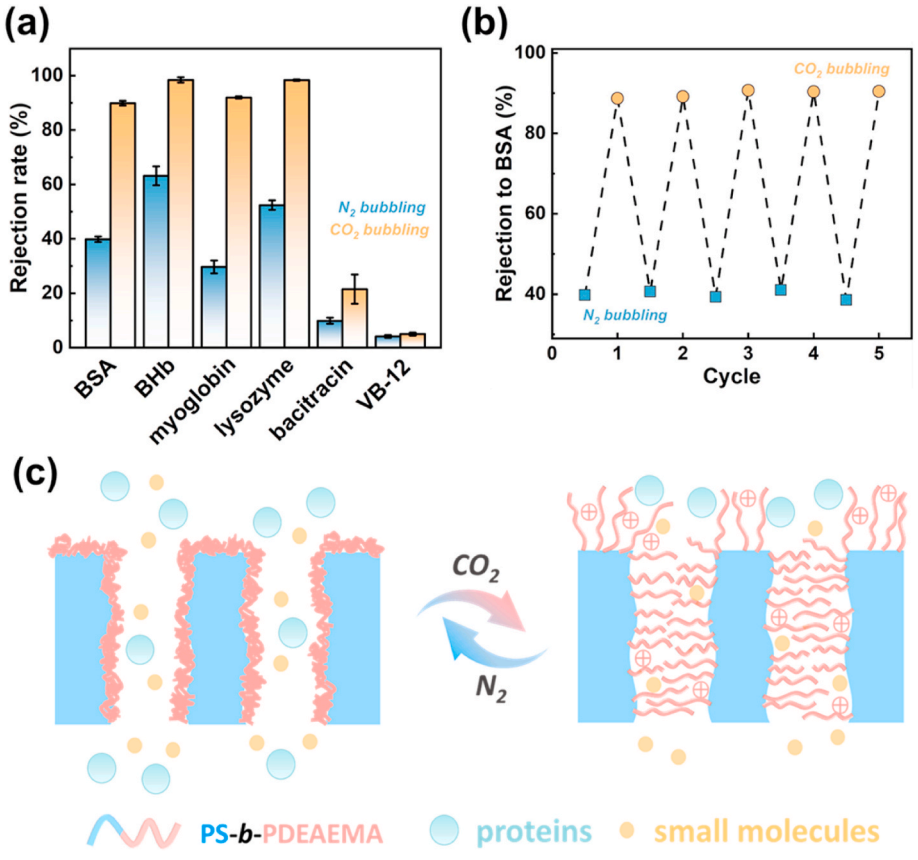

Fig. 6. (a) Rejections to different biomolecules under CO_2 and N_2 stimulation. (b) Rejections to BSA under alternating CO_2/N_2 stimulation. (c) Schematic of the regulation on separation performances of membranes by CO_2/N_2 stimulation.

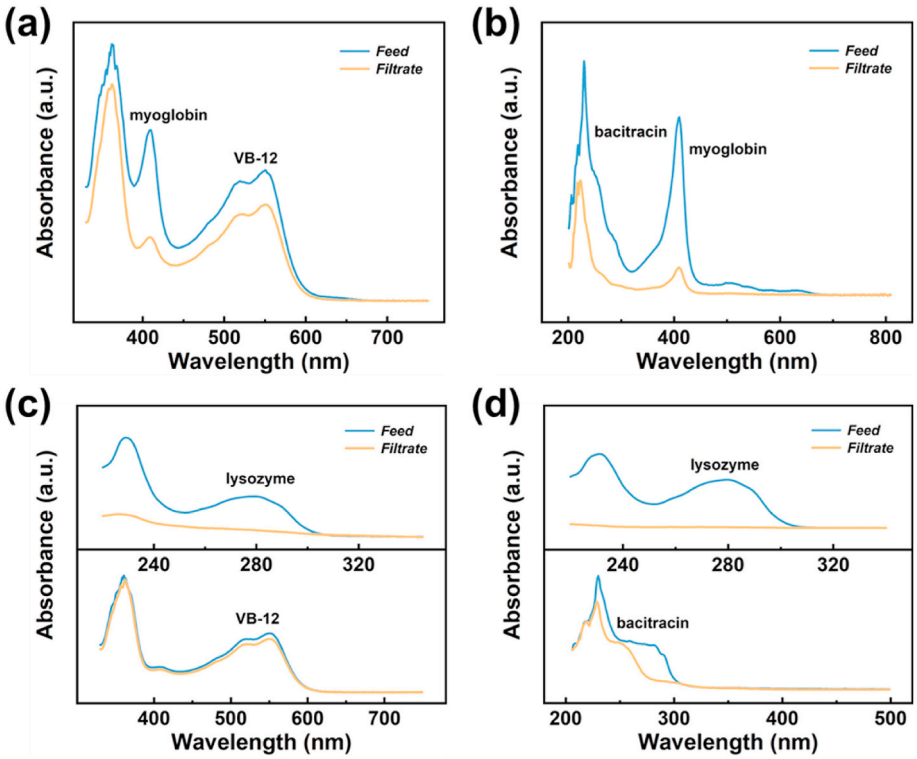

Fig. 7. The UV–vis absorption spectra of mixed systems: (a) VB-12/myoglobin, (b) bacitracin/myoglobin, (c) VB-12/lysozyme, and (d) bacitracin/lysozyme.

according to Eq. (5), and the results were 93.4%, 88.7%, 95.5%, 97%, respectively. The high separation efficiencies confirm the excellent selective sieving capabilities of the membrane to separate macromolecular proteins and small molecules upon CO_2 stimulation.

4. Conclusion

In summary, we fabricate the CO_2-responsive membranes from a block copolymer of PDEAEMA-*b*-PS by using the selective swelling method. The swelling behaviors of PDEAEMA-*b*-PS are investigated, demonstrating it is convenient to obtain nanoporous structures via selective swelling and the pore sizes and porosities are adjustable simply by changing the swelling durations. The spectroscopic ellipsometry monitors the thickness change of PDEAEMA-*b*-PS films in situ, manifesting the conformation transformation of PDEAEMA chains from the collapsed state to the stretched state upon CO_2 stimulation. Also, the surface hydrophilicity-hydrophobicity transition of films is realized by manipulating CO_2/N_2 treatment, due to the protonation/deprotonation behaviors of PDMAEMA chains. Based on these properties, water permeances of PDEAEMA-*b*-PS membranes can be reversibly switched in the range of about 100–2100 $L{\cdot}m^{-2}{\cdot}h^{-1}{\cdot}bar^{-1}$ upon cycles of CO_2/N_2 alternation, and exhibit great cyclic responsiveness. Rejection tests show the membranes are capable to reject varied proteins in the presence of CO_2, while allow their transport upon N_2 stimulation, displaying the function as the proteins "on-off" gate. Furthermore, separation tests demonstrate the membranes have high separation efficiencies for the mixtures of VB-12/myoglobin, bacitracin/myoglobin, VB-12/lysozyme and bacitracin/lysozyme, which are 93.4%, 88.7%, 95.5%, 97%, respectively. Therefore, the CO_2-responsive membranes developed in this work have great prospects for controllable biomolecules separation applications.

Author statement

Xiangyue Ye: Methodology, Investigation, Writing-Original Draft, Jiemei Zhou: Methodology, Writing-Review & Editing, Chenxu Zhang: Investigation, Yong Wang: Supervision, Conceptualization.

Declaration of competing interest

The authors declare that they have no known competing financial interests or personal relationships that could have appeared to influence the work reported in this paper.

Data availability

No data was used for the research described in the article.

Acknowledgments

Financial support from the Natural Science Foundation of Jiangsu Province (BK20190671), and the National Natural Science Foundation of China (21908095, 21825803) is gratefully acknowledged.

Appendix A. Supplementary data

Supplementary data to this article can be found online at https://doi.org/10.1016/j.memsci.2022.121022.

References

[1] W. Wang, P.F. Li, R. Xie, X.J. Ju, Z. Liu, L.Y. Chu, Designable micro-/nano-structured smart polymeric materials, Adv. Mater. (2022), 2107877.
[2] S. Samadzadeh, M. Babazadeh, N. Zarghami, Y. Pilehvar-Soltanahmadi, H. Mousazadeh, An implantable smart hyperthermia nanofiber with switchable, controlled and sustained drug release: possible application in prevention of cancer local recurrence, Mater. Sci. Eng., C 118 (2021), 111384.
[3] Y. Zhu, M. Zhang, S. Wei, B. Wang, J. He, X. Qiu, Temperature-responsive P (NIPAM-co-NHMA)-grafted organic-inorganic hybrid hollow mesoporous silica nanoparticles for controlled drug delivery, J. Drug Deliv. Sci. Technol. 70 (2022), 103197.
[4] C. Ma, W. Lu, X. Yang, J. He, X. Le, L. Wang, J. Zhang, M.J. Serpe, Y. Huang, T. Chen, Bioinspired anisotropic hydrogel actuators with on–off switchable and color-tunable fluorescence behaviors, Adv. Funct. Mater. 28 (2018), 1704568.

[5] C.W. Lin, S. Xue, C. Ji, S.C.A. Huang, V. Tung, R.B. Kaner, Conducting polyaniline for antifouling ultrafiltration membranes: solutions and challenges, Nano Lett. 21 (2021) 3699–3707.

[6] Y. Shao, L. Zhou, C. Bao, J. Ma, M. Liu, F. Wang, Magnetic responsive metal–organic frameworks nanosphere with core–shell structure for highly efficient removal of methylene blue, Chem. Eng. J. 283 (2016) 1127–1136.

[7] T. Tripathi, M. Kamaz, S.R. Wickramasinghe, A. Sengupta, Designing electric field responsive ultrafiltration membranes by controlled grafting of poly (ionic liquid) brush, Int. J. Environ. Res. Publ. Health 17 (2020) 271–284.

[8] J. Lin, J. Hu, W. Wang, K. Liu, C. Zhou, Z. Liu, S. Kong, S. Lin, Y. Deng, Z. Guo, Thermo and light-responsive strategies of smart titanium-containing composite material surface for enhancing bacterially anti-adhesive property, Chem. Eng. J. 407 (2021), 125783.

[9] H. Che, M. Huo, L. Peng, T. Fang, N. Liu, L. Feng, Y. Wei, J. Yuan, CO2 -responsive nanofibrous membranes with switchable oil/water wettability, Angew. Chem. Int. Ed. 54 (2015) 8934–8938.

[10] L. Dong, W. Fan, H. Zhang, M. Chen, Y. Zhao, CO2-responsive polymer membranes with gas-tunable pore size, Chem. Commun. 53 (2017) 9574–9577.

[11] F. Chen, F. Zhang, Y. Wang, J. Peng, L. Cao, Q. Mei, M. Ge, L. Li, M. Chen, W. Dong, Z. Chang, Biomimetic redox-responsive mesoporous organosilica nanoparticles enhance cisplatin-based chemotherapy, Front. Bioeng. Biotechnol. 10 (2022), 860949.

[12] N. Amaly, A.Y. El-Moghazy, G. Sun, Fabrication of polydopamine-based NIR-light responsive imprinted nanofibrous membrane for effective lysozyme extraction and controlled release from chicken egg white, Food Chem. 357 (2021), 129613.

[13] Y. Chen, J. Qiu, X. Zhang, H. Wang, W. Yao, Z. Li, Q. Xia, G. Zhu, J. Wang, A visible light/heat responsive covalent organic framework for highly efficient and switchable proton conductivity, Chem. Sci. 13 (2022) 5964–5972.

[14] Z. Yaghoubi, J.B. Parsa, Preparation of thermo-responsive PNIPAAm-MWCNT membranes and evaluation of its antifouling properties in dairy wastewater, Mater. Sci. Eng., C 103 (2019), 109779.

[15] N. Gao, L. Wang, Y. Zhang, F. Liang, Y. Fan, Modified ceramic membrane with pH/ethanol induced switchable superwettability for antifouling separation of oil-in-acidic water emulsions, Separ. Purif. Technol. 293 (2022), 121022.

[16] Q. Ye, R. Wang, C. Chen, B. Chen, X. Zhu, High-flux pH-responsive ultrafiltration membrane for efficient nanoparticle fractionation, ACS Appl. Mater. Interfaces 13 (2021) 56575–56583.

[17] A.U. Alrayyes, Y. Hu, R.F. Tabor, H. Wang, K. Saito, Photo-switchable membranes constructed from graphene oxide/star-PDMS nanocomposites for gas permeation control, J. Mater. Chem. 9 (2021) 21167–21174.

[18] Z. Meng, J. Zhai, Synthesis, functionalization and application of stimuli-responsive polymer porous membranes, Curr. Org. Chem. 22 (2018) 737–749.

[19] B. Saini, D. Vaghani, S. Khuntia, M.K. Sinha, A. Patel, R. Pindoria, A novel stimuli-responsive and fouling resistant PVDF ultrafiltration membrane prepared by using amphiphilic copolymer of poly(vinylidene fluoride) and poly(2-N-morpholino) ethyl methacrylate, J. Membr. Sci. 603 (2020), 118047.

[20] Y. Wang, C. Liu, D. Shi, L. Dong, M. Chen, W. Dong, Thermo-responsive membranes fabricated by immobilization of microgels with enhanced gating coefficient and reversible behavior, Compos. Commun. 27 (2021), 100840.

[21] R. Wei, F. Yang, R. Gu, Q. Liu, J. Zhou, X. Zhang, W. Zhao, C. Zhao, Design of robust thermal and anion dual-responsive membranes with switchable response temperature, ACS Appl. Mater. Interfaces 10 (2018) 36443–36455.

[22] M.S. Oak, T. Kobayashi, H.Y. Wang, T. Fukaya, N. Fujii, pH effect on molecular size exclusion of polyacrylonitrile ultrafiltration membranes having carboxylic acid groups, J. Membr. Sci. 123 (1997) 185–195.

[23] B.X. Yang, X. Yang, B.C. Liu, Z.Q. Chen, C. Chen, S.M. Liang, L.Y. Chu, J. Crittenden, PVDF blended PVDF-g-PMAA pH-responsive membrane: effect of additives and solvents on membrane properties and performance, J. Membr. Sci. 541 (2017) 558–566.

[24] Q. Shi, Y.L. Su, X. Ning, W.J. Chen, J.M. Peng, Z.Y. Jiang, Graft polymerization of methacrylic acid onto polyethersulfone for potential pH-responsive membrane materials, J. Membr. Sci. 347 (2010) 62–68.

[25] X. Shi, Z. Xu, C. Huang, Y. Wang, Z. Cui, Selective swelling of electrospun block copolymers: from perforated nanofibers to high flux and responsive ultrafiltration membranes, Macromolecules 51 (2018) 2283–2292.

[26] X.Y. Qiu, H.Z. Yu, K.V. Peinemann, Selective separation of similarly sized proteins with tunable nanoporous block copolymer membranes, Procedia Eng. 44 (2012) 461–463.

[27] L. Dong, Y. Zhao, CO2-switchable membranes: structures, functions, and separation applications in aqueous medium, J. Mater. Chem. 8 (2020) 16738–16746.

[28] Q. Zhang, Z.W. Wang, L. Lei, J. Tang, J.L. Wang, S.P. Zhu*, CO2-switchable membranes prepared by immobilization of CO2-breathing microgels, ACS Appl. Mater. Interfaces 9 (2017) 44146–44151.

[29] C. Zhang, J. Zhou*, X. Ye, Z. Li, Y. Wang*, CO2-responsive membranes prepared by selective swelling of block copolymers and their behaviors in protein ultrafiltration, J. Membr. Sci. 641 (2022), 119928.

[30] H. Yu, X. Qiu, S.P. Nunes, K.V. Peinemann, Self-assembled isoporous block copolymer membranes with tuned pore sizes, Angew. Chem. Int. Ed. 53 (2014) 10072–10076.

[31] G.D. Zhu, Y.R. Ying, X. Li, Y. Liu, C.Y. Yang, Z. Yi, C.J. Gao, Isoporous membranes with sub-10 nm pores prepared from supramolecular interaction facilitated block copolymer assembly and application for protein separation, J. Membr. Sci. 566 (2018) 25–34.

[32] Y. Liao, M. Tian, R. Wang, A high-performance and robust membrane with switchable super-wettability for oil/water separation under ultralow pressure, J. Membr. Sci. 543 (2017) 123–132.

[33] R. Li, J. Xu, T. Wang, L. Wang, F. Li, S. Liu, X. Jiang, Q. Luo, J. Liu, Dynamically tunable ultrathin protein membranes for controlled molecular separation, ACS Appl. Mater. Interfaces 13 (2021) 12359–12365.

[34] J. Zhou, C. Zhang, C. Shen, Y. Wang, Synthesis of poly(2-dimethylaminoethyl methacrylate)-block- poly(styrene-alt-N-phenylmaleimide) and its thermo-tolerant nanoporous films prepared by selective swelling, Polymer 164 (2019) 126–133.

[35] Y. Wang, Nondestructive creation of ordered nanopores by selective swelling of block copolymers: toward homoporous membranes, Acc. Chem. Res. 49 (2016) 1401–1408.

[36] N. Yan, Y. Wang, Selective swelling induced pore generation of amphiphilic block copolymers: the role of swelling agents, J. Polym. Sci. B Polym. Phys. 54 (2016) 926–933.

[37] H. Yang, L. Guo, Z. Wang, N. Yan, Y. Wang, Nanoporous films with superior resistance to protein adsorption by selective swelling of polystyrene-block-poly (ethylene oxide), Ind. Eng. Chem. Res. 55 (2016) 8133–8140.

[38] Z. Wang, R. Liu, H. Yang, Y. Wang, Nanoporous polysulfones with in situ PEGylated surfaces by a simple swelling strategy using paired solvents, Chem. Commun. 53 (2017) 9105–9108.

[39] L. Dong, W. Fan, X. Tong, H. Zhang, M. Chen, Y. Zhao, A CO2-responsive graphene oxide/polymer composite nanofiltration membrane for water purification, J. Mater. Chem. 6 (2018) 6785–6791.

[40] J. Zhang, Y. Liu, J. Guo, Y. Yu, Y. Li, X. Zhang, A CO2-responsive PAN/PAN-co-PDEAEMA membrane capable of cleaning protein foulant without the aid of chemical agents, React. Funct. Polym. 149 (2020), 104503.

[41] J. Wang, H. Guan, Q. Liang, M. Ding, Construction of copper (II) affinity- DTPA functionalized magnetic composite for efficient adsorption and specific separation of bovine hemoglobin from bovine serum, Compos. B Eng. 198 (2020), 108248.

[42] N. Jia, Y. Wen, G. Yang, Q. Lian, C. Xu, H. Shen, Direct electrochemistry and enzymatic activity of hemoglobin immobilized in ordered mesoporous titanium oxide matrix, Electrochem. Commun. 10 (2008) 774–777.

[43] S. Jaag, M. Shirokikh, M. Lammerhofer, Charge variant analysis of protein-based biopharmaceuticals using two-dimensional liquid chromatography hyphenated to mass spectrometry, J. Chromatogr. A 1636 (2021), 461786.

[44] Y. Huang, P. Yang, F. Yang, C. Chang, Self-supported nanoporous lysozyme/nanocellulose membranes for multifunctional wastewater purification, J. Membr. Sci. 635 (2021), 119537.

[45] M.S. Bhattacharyya, P. Hiwale, M. Piras, L. Medda, D. Steri, M. Piludu, A. Salis, M. Monduzzi, Lysozyme adsorption and release from ordered mesoporous materials, J. Phys. Chem. C 114 (2010) 19928–19934.

[46] O. Willemsen, E. Machtejevas, K.K. Unger, Enrichment of proteinaceous materials on a strong cation-exchange diol silica restricted access material: protein-protein displacement and interaction effects, J. Chromatogr. A 1025 (2004) 209–216.

[47] Z.K. Li, Y. Wei, X. Gao, L. Ding, Z. Lu, J. Deng, X. Yang, J. Caro, H. Wang, Antibiotics separation with mxene membranes based on regularly stacked high-aspect-ratio nanosheets, Angew. Chem. Int. Ed. 59 (2020) 9751–9756.

[48] Z. Zhang, C. Yin, X. Shi, G. Yang, Y. Wang, Masking covalent organic frameworks (COFs) with loose polyamide networks for precise nanofiltration, Separ. Purif. Technol. 283 (2022), 120233.

[49] T. Matsumoto, H. Inoue, Small angle x-ray scattering and viscoelastic studies of the molecular shape and colloidal structure of bovine and rat serum albumins in aqueous systems, Chem. Phys. 178 (1993) 591–598.

[50] M. Zhang, D. Cheng, X.W. He, L.X. Chen, Y.K. Zhang, Magnetic silica-coated sub-microspheres with immobilized metal ions for the selective removal of bovine hemoglobin from bovine blood, Chem. Asian J. 5 (2010) 1332–1340.